

Effects of Polariton Energy Renormalisation in the Microcavity Optical Parametric Oscillator

D. M. Whittaker

Department of Physics and Astronomy, University of Sheffield, Sheffield, S3 7RH, United Kingdom.

(Dated: January 4, 2022)

The CW microcavity optical parametric oscillator (OPO) state is investigated using a theoretical treatment which includes the contributions of the pump, signal and idler populations to the renormalisation of the polariton energies (the ‘blue-shift’). The theory predicts the pumping conditions under which the OPO switches on, showing that a pump angle $>\sim 10^\circ$ is required, but there is no particular significance to the ‘magic-angle’ where pump, signal and idler are all on resonance. The signal and idler renormalisation contributions also causes the signal emission to be driven towards the normal direction as the pump power increases above threshold.

The behaviour of a resonantly pumped semiconductor microcavity can be best described using the terminology of the optical parametric oscillator (OPO): with pumping above threshold at finite angle, a coherent signal appears, close to the normal direction, accompanied by an idler on the other side of the pump.^{1,2} However, this is an unusual OPO, as the nonlinearity is χ^3 , rather than the typical χ^2 . One consequence is that there is a self-interaction, the ‘blue-shift’, which can be thought of as a renormalisation of the polariton energies. This renormalisation obviously depends on the pump, signal and idler populations. However, although the term has been discussed in previous theoretical work, its effect on the OPO state have been ignored, or only the pump contribution has been considered. The purpose of the present paper is to show that, when the renormalisation is properly treated, a number of puzzling aspects of the experimental results can be explained.

Recent experiments³ have shown that the CW-OPO can be switched on for a range of pump angles and energies, from 10° to at least 24° , with relatively small changes in threshold. This CW situation contrasts with the ultra-fast behaviour, where the response is strongly peaked about a ‘magic-angle’, of $\sim 16^\circ$, when the pump, signal and idler all lie on the polariton dispersion.^{4,5} By investigating the stability of a state in which only the pump polariton is occupied, the theoretical treatment with the self-interaction provides a prediction of values of the pump angle, power and energy at which the OPO can occur. In fact, the OPO is not the only instability of the system: a simple bistable behaviour can also be obtained, as observed experimentally by Baas *et al*⁸ for normal incidence pumping. The theory predicts that for small pump angles, only bistability occurs, while for angles greater than $\sim 10^\circ$ the OPO switches on. Furthermore, the OPO threshold is found to vary smoothly with pump angle and energy, giving no special significance to the magic angle.

The other aspect of the experimental behaviour which is addressed here concerns the direction of the emerging signal, which is always found to be within a few degrees of the surface normal, whatever the angle of the pump. This is surprising because, if the signal angle were simply determined by the requirement that the mismatch of the signal and idler energies from the polariton dispersion is minimised, a wider range of angles would be obtained, depending on the pump energy and angle. The present theory predicts that this will in fact happen, but only very close to the threshold: at higher pump powers the renormalisation contributions from the signal and idler switch off the high angle OPO and pull the small angle states into resonance. In a theory without these contributions, the pump population is pinned to its threshold value, so nothing can change at higher pump powers.

The first theoretical models of the microcavity OPO^{6,7} showed that the polariton energy renormalisation arises naturally from a description in terms of exciton-exciton scattering⁶ or a χ^3 nonlinearity.⁷ Although the renormalisation was derived, its effects were not included in the solution for the OPO states. The renormalisation of the pump polariton state was shown by Baas *et al*⁸ to explain the observed bistability, but this treatment was not extended to consider the OPO state. Gippius *et al*⁹ discuss the bistability and OPO instability, making comparisons with a numerical model, including a continuum of modes, from which emerges the property of emission close to the normal. The present work is an analytic treatment which provides a physical explanation for the numerical and experimental results, by including the contributions to the renormalisation from the signal and idler populations in the description of the OPO.

The treatment assumes that the pump beam is spatially uniform, and the pump, signal and idler fields are simple plane waves. Although this is not fully realistic, as all experiments use a finite spot, it should give reasonable results for illumination with gradual spatial intensity variations. As will be discussed below, some differences between the theoretical predictions and experiment are probably due to the effects of spatially inhomogeneous pumping. It should also be noted that even for uniform pumping, it is possible that there are solutions with spatial structure to the internal fields.

The theoretical expressions derived in this paper are fully two-dimensional, valid for any in-plane wave-vectors consistent with momentum conservation. However, for simplicity, the results presented in the figures assume the

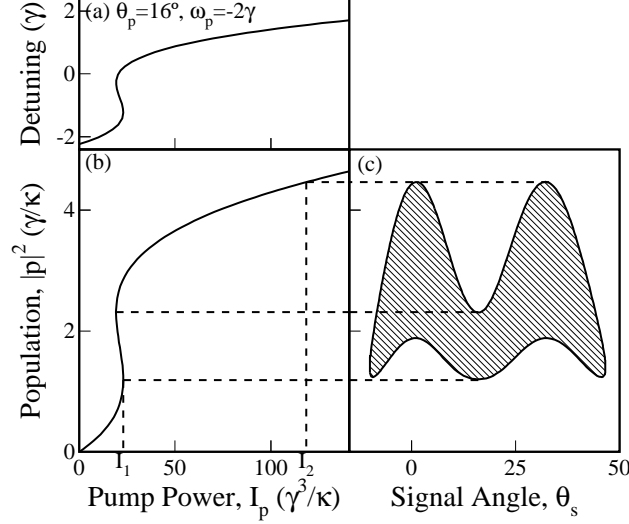


FIG. 1: The pump-only state for $\theta_p = 16^\circ$, $\omega_p = -2\gamma$. (a) Detuning of the pump relative to the polariton energy, including the renormalisation contribution. (b) S-curve showing the relationship between the pump polariton population $|p|^2$ and the external pump power I_p . (c) Values of $|p|^2$ (shaded region) for which the pump-only state is unstable, as a function of the signal angle, θ_s . I_1 and I_2 are the pump powers corresponding to the lowest and highest unstable values of $|p|^2$ for any θ_s : the OPO switches on when $I_2 > I_1$.

pump, signal and idler lie on a line passing through $k = 0$ in wave-vector space, and the excitations considered in the stability treatments are similarly confined. Calculations have also been made without this restriction, and stable OPO states which do not quite fall on such a radial line can be found. Similarly, extending the stability treatment to consider all excitations tends to reduce slightly the stability ranges of the solutions described.

The remainder of the paper is developed in the following way: In Section I, the state with only pump polariton mode occupied is described, and its stability is investigated, leading to a criterion for determining the conditions under which the OPO switches on. In Section II, the model of the OPO state with finite amplitude is derived, showing how the emission is pulled towards the normal direction. Finally, in Sections III and IV the OPO state stability is investigated, and the various predictions of the model are discussed.

I. THE PUMP STATE

This section describes a state in which only a single, pumped polariton mode is populated. The conditions under which this state becomes unstable are derived, and criteria are obtained for determining whether a simple bistability results, or the OPO switches on.

The pump mode is assumed to be a plane wave $\phi_p = (p/|X_p|^2) \exp i(k_p x - \omega_p t)$, where the amplitude, p , satisfies:⁷

$$\frac{1}{|X_p|^2}(\omega_0(k_p) - i\gamma_p - \omega_p)p + \kappa|p|^2 p = \frac{|C_p|}{|X_p|} f_p. \quad (1)$$

Here, $\omega_0(k_p)$ is the lower branch dispersion at the pump wave-vector, γ_p its width, $|C_p|$ and $|X_p|$ the cavity and exciton amplitudes (Hopfield factors), and f_p the external pump amplitude. The non-linear term, $\kappa|p|^2 p$ represents the self interaction of the pump polaritons. By appropriate scaling of the fields,⁷ the coefficient κ can be made equal to unity, which forthwith is taken to be the case. The use of this single-branch form assumes that the polariton coupling is sufficiently large that the two branches are not mixed by the non-linear terms.

The solution of the cubic Eq.1 has been discussed in Ref(8): when the detuning $\omega_p - \omega_0(k_p) > \sqrt{3}\gamma_p$, the cubic has two turning points, resulting in a characteristic S-curve, as shown in Fig.1(b)¹¹. For pump-powers falling between the two turning points, the system is bistable (the branch with negative slope is unstable). Fig.1(a) shows how this bistability is intimately linked with the zero-crossing of the pump detuning, as it changes due to the blue-shift

contributions. For negative detunings, the shift pulls the polariton feature towards resonance with the pump, causing the population to grow super-linearly. However, when the detuning becomes positive, the polariton is pushed away from resonance. The pump polariton population must lie on this curve if only the pump mode is significantly occupied. However, if other modes have finite occupation, as in the OPO state, this restriction no longer applies. Hence the conditions under which the OPO switches on can be found by determining which parts of the pump-only curve are unstable.

The stability of the pump-only state is determined by considering the spectrum of small excitations with frequency ω and wave-vector q , of the form

$$\phi_p = e^{i(k_p x - \omega_p t)} \left[p + s e^{-i(qx - \omega t)} + i e^{i(qx - \omega^* t)} \right] \quad (2)$$

which describes signal and idler modes with amplitudes s , i , and wave-vector/energies ($k_s = k_p - q$, $\omega_s = \omega_p - \omega$) and ($k_i = k_p + q$, $\omega_i = \omega_p + \omega$). Expanding to first order in s and i , this gives

$$\frac{1}{|X_s|^2} (\omega_0(k_s) - i\gamma_s - \omega_p + \omega) s + 2|p|^2 s + p^2 i^* = 0 \quad (3a)$$

$$\frac{1}{|X_i|^2} (\omega_0(k_i) - i\gamma_i - \omega_p - \omega^*) i + 2|p|^2 i + p^2 s^* = 0 \quad (3b)$$

Considering these equations as an eigenproblem for the amplitudes s and i^* , the complex eigenvalues, ω , are given by the condition that the determinant of the coefficients is zero, that is

$$\begin{aligned} & (\omega_0(k_s) - i\gamma_s - \omega_p + \omega + 2|X_s|^2|p|^2) \times \\ & (\omega_0(k_i) + i\gamma_i - \omega_p - \omega + 2|X_i|^2|p|^2) = |X_s|^2|X_i|^2|p|^4 \end{aligned} \quad (4)$$

The threshold for instability corresponds to $\text{Im}\{\omega\} = 0$, which occurs when

$$\Delta^2 + \Gamma^2 = \frac{\Gamma^2}{\gamma_s \gamma_i} |X_s|^2 |X_i|^2 |p|^4, \quad (5)$$

where $\Gamma = \gamma_s + \gamma_i$ and

$$\Delta = \omega_0(k_s) + \omega_0(k_i) - 2\omega_p + 2(|X_s|^2 + |X_i|^2)|p|^2 \quad (6)$$

is the mismatch from the resonance condition $2\omega_p = \omega_0(k_s) + \omega_0(k_i)$, modified by the blue-shift. Eqs. (5) and (6) provide a quadratic condition for $|p|^2$ at the boundary of the instability region.

Fig.1(c) shows the instability region, plotted as a function of the signal angle θ_s . For $\theta_s = \theta_p$, the extrema of the instability region correspond to the two turning points of the S-curve, so this analysis correctly predicts that the negative-slope portion of the curve is unstable. However, for the pumping conditions shown, the total extent of the instability region for all θ_s is significantly greater: converting the extremal $|p|^2$ values to pump powers gives a range between I_1 and I_2 on Fig.1(b), for which the pump-only state is unstable.

The discussion above provides a criterion for determining whether the OPO state turns on for a given pump angle and energy: if there is a range of pump powers I_p for which the pump-only state is unstable, something more complicated, presumably the OPO, must turn on in between. In terms of Fig.1(b), this means that $I_2 > I_1$. If, on the other hand, $I_2 < I_1$, the system can jump straight from the lower branch of the S-curve to a stable state on the upper branch, and a simple bistability occurs. Of course, this does not rule out the possibility of the OPO switching on, but numerical experiments similar to those described in Ref.(9) only produce bistability.¹⁰ A further possibility is that there is no unstable region, and $|p|^2$ simply rises smoothly with increasing pump-power. Note that the OPO state does not require a bistable S-curve, as the unstable region of Fig.1(c) does not have to include $\theta_s = \theta_p$.

In Fig.2, the sectors of (θ_p, ω_p) corresponding to these three types of behaviour are delineated. The figure shows that there is a minimum pump angle, $\sim 10^\circ$, below which it is not possible to turn the OPO on. In the OPO sector, the threshold rises monotonically with increasing θ_p and ω_p , and there is no special significance to the ‘magic angle’, $\theta_p \sim 16^\circ$, at which the pump, signal and idler can all be made resonant with the lower branch dispersion. These conclusions are broadly consistent with the experimental results of Butté *et al*³.

The key property which determines whether the OPO switches on appears to be the presence of a minimum in the higher threshold for $\theta_s = \theta_p$, as in Fig.1(c). If this is the case, the upper threshold, I_2 , is shifted above the higher knee in the S-curve, providing a gap in the stability of the pump-only curve. In Fig.3, it is shown that this correlates with the presence of a maximum in the θ_s dependence of the bare mismatch when $\theta_s = \theta_p$: for $\theta_p < 10^\circ$, instead there is a minimum for this value of θ_s .

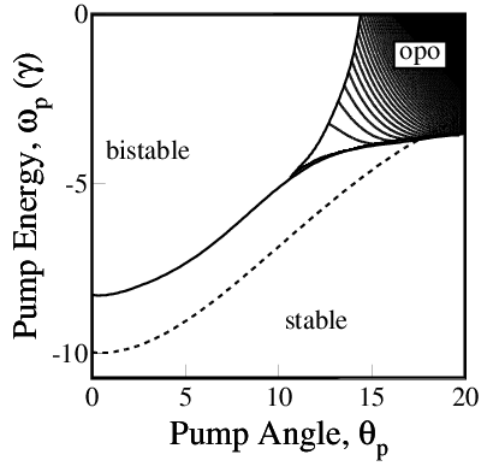


FIG. 2: Division of the (θ_p, ω_p) plane into sectors of different behaviour. In the ‘stable’ region, as the pump power, I_p rises, the pump population, $|p|^2$, increases smoothly. In the bistable region, there is a discontinuous jump in $|p|^2$, but no other state becomes occupied. The contours in the OPO region show the variation in the threshold, increasing in steps of $10(\gamma^3/\kappa)$ from the bottom left to the top right. The bare polariton dispersion is shown as a dashed line.

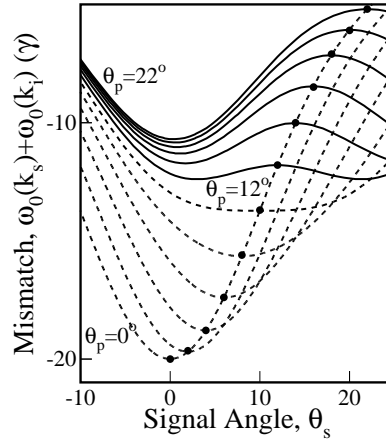


FIG. 3: The bare mismatch, $\omega_0(k_s) + \omega_0(k_i)$, plotted as a function of signal angle, θ_s , for different values of pump angle, θ_p . The filled circles indicate the points where $\theta_s = \theta_p$. For $\theta_p < 12^\circ$, the dashed curves, these points are minima and there is no OPO. For $\theta_p \geq 12^\circ$, they are maxima, and the OPO switches on. In this regime, the minimum mismatch always occurs close to $\theta_s = 0^\circ$.

II. THE OPO STATES

The previous section described the OPO states at threshold, when the signal and idler populations are still zero. In this section, the treatment is extended to include contributions of finite signal and idler populations to the dispersion renormalisation. This model is solved to obtain the variation of the pump, signal and idler populations above threshold for a range of signal angles.

Eqs. (2), (3a) and (3b) are only accurate to first order in s and i . For finite signal and idler populations, they are modified to include the renormalisation effects of the signal and idler populations, and the depletion of the pump:

$$\frac{1}{|X_p|^2}(\omega_0(k_p) - i\gamma_p - \omega_p)p + (|p|^2 + 2|s|^2 + 2|i|^2)p + 2p^*si = \frac{|C_p|}{|X_p|}f_p \quad (7a)$$

$$\frac{1}{|X_s|^2}(\omega_0(k_s) - i\gamma_s - \omega_s)s + (2|p|^2 + |s|^2 + 2|i|^2)s + p^2i^* = 0 \quad (7b)$$

$$\frac{1}{|X_i|^2}(\omega_0(k_i) - i\gamma_i - \omega_i)i + (2|p|^2 + 2|s|^2 + |i|^2)i + p^2s^* = 0. \quad (7c)$$

Note the different form for the renormalisation of each state: the self-interaction term has only half the strength of each cross term. In the OPO state the renormalisation does *not* produce a uniform blue-shift of the polariton dispersion.

With the condition that ω_s and $\omega_i = 2\omega_p - \omega_s$ must be real, Eqs.(7b,7c) require

$$\omega_s = \frac{\gamma_i}{\Gamma} [\omega_0(k_s) + |X_s|^2(2|p|^2 + |s|^2 + 2|i|^2)] \quad (8)$$

and for this value of ω_s

$$\frac{|s|^2}{|i|^2} = \frac{|X_s|^2\gamma_i}{|X_i|^2\gamma_s} \quad (9)$$

Then $|p|^2$, $|s|^2$ and $|i|^2$ satisfy Eq.5 with the mismatch modified to include the signal and idler contributions to the renormalisation,

$$\begin{aligned} \Delta = & \omega_0(k_s) + \omega_0(k_i) - 2\omega_p + |X_s|^2(2|p|^2 + |s|^2 + 2|i|^2) \\ & + |X_i|^2(2|p|^2 + 2|s|^2 + |i|^2), \end{aligned} \quad (10)$$

which, using Eq.9, represents a biquadratic equation connecting $|p|^2$ and $|s|^2$. A further relationship between the two variables can be obtained by solving Eq.7c for i in terms of s^* , and substituting in the pump equation (7a) to get

$$\begin{aligned} \frac{1}{|X_p|^2}(\omega_0(k_p) - i\gamma_p - \omega_p)p + (|p|^2 + 2|s|^2 + 2|i|^2)p \\ - 2|X_i|^2 \frac{\Gamma}{\gamma_i} \frac{|s|^2|p|^2}{\Delta + i\Gamma} = \frac{|C_p|}{|X_p|}f_p. \end{aligned} \quad (11)$$

These two relationships can readily be solved to obtain the values of $|p|^2$ and $|s|^2$ in the OPO states, including the contributions of the signal and idler populations to the blueshifts.

Such solutions for the OPO state are shown in Fig.4. Above threshold, there is generally a region where the pump population, $|p|^2$, remains nearly flat, while the signal, $|s|^2$, increases with pump power. In a treatment with just the pump contribution to the renormalisation, $|p|^2$ would be completely flat for all powers above threshold. However, in the present model, a power is reached where the flat behaviour ceases, and $|p|^2$ increases rapidly towards the pump-only line, at which point the OPO switches off, with $|s|^2$ falling to zero. Examining the curves for different pump angles θ_s reveals that the maximum I_p at the turn-over occurs when $\theta_s \sim 1^\circ$, and it decreases rapidly on either side, so at -7° and $+9^\circ$ there is only a small range of I_p in which the OPO state exists.

The origin of this behaviour can be understood by considering the mismatch Δ , from Eq.10, which is zero when the pump and the renormalised signal and idler satisfy the triple resonance condition. As is shown in Fig.4(b), Δ is negative in the flat region, where the increasing blue-shift is thus pulling the OPO towards resonance, and helping the signal to increase. The turn-over occurs around the pump power where Δ becomes positive, so increases in the blue-shift drive the system away from resonance, and the OPO rapidly turns off. The dependence on signal angle is therefore a consequence of the different values of the bare mismatch $\omega_0(k_s) + \omega_0(k_i) - 2\omega_p$, which, because of the dispersion shape, always has its minimum close to $\theta_s = 0$. Indeed, it can be seen from Fig.3 that this occurs at approximately $+1^\circ$ for $\theta_p = 16^\circ$, and changes very little over the range of pump angles for which the OPO switches on. Thus, though the signal angle with the smallest bare-mismatch has a lower threshold, when the pump power is increased the growing blue-shift quickly switches that state off and the signal moves towards $\theta_s = 0$.

III. OPO STABILITY

The solutions for the OPO states described in the previous section are only of physical relevance if they are stable. This section describes a linear stability analysis of the OPO, and shows that there are stable solutions, but they become unstable when the pump population curves on Fig.4 turn over.

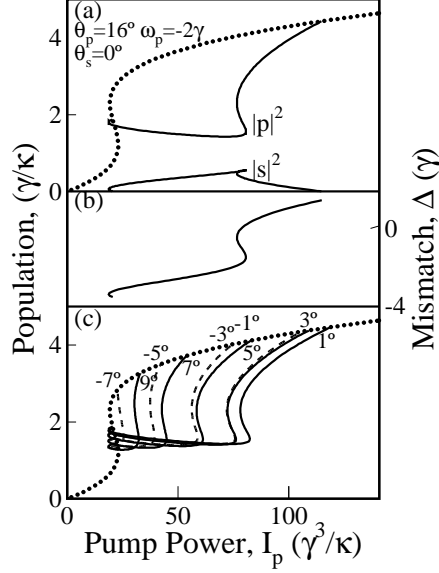


FIG. 4: The OPO states including signal and idler renormalisation contributions. (a) Relationship between the pump population, $|p|^2$, and pump power, I_p , for signal angle $\theta_s = 0$, and the corresponding signal population $|s|^2$. (b) The mismatch Δ from Eq.10 as a function of I_p for $\theta_s = 0$. (c) The pump population variation, as in (a), for a number of values of θ_s . The curves for negative values of θ_s are shown dashed for clarity.

The stability analysis for the OPO proceeds in a similar manner to that for the pump-only state. The spectrum of small excitations about the OPO state is calculated using a linearised expansion of fluctuations in the pump, signal and idler modes. For an excitation wave-vector q and frequency ω , these fluctuations satisfy a set of coupled equations, from which the dispersion is obtained using the condition that the determinant of the coefficients is zero. Thus

$$\begin{vmatrix} d_p & p^2 + 2si & 2(ps^* + p^*i) & 2ps & 2(p^*s + pi^*) & 2pi \\ p^{*2} + 2s^*i^* & \bar{d}_p & 2p^*s^* & 2(p^*s + pi^*) & 2p^*i^* & 2(ps^* + p^*i) \\ 2(p^*s + pi^*) & 2ps & d_s & s^2 & 2si^* & p^2 + 2si \\ 2p^*s^* & 2(ps^* + p^*i) & s^{*2} & \bar{d}_s & p^{*2} + 2s^*i^* & 2s^*i^* \\ 2(ps^* + p^*i) & 2pi & 2s^*i & p^2 + 2si & d_i & i^2 \\ 2p^*i^* & 2(p^*s + pi^*) & p^{*2} + 2s^*i^* & 2si^* & i^{*2} & \bar{d}_i \end{vmatrix} = 0 \quad (12)$$

where

$$\begin{aligned} d_p &= \frac{1}{|X_p|^2}(\omega_0(k_p - q) - i\gamma_p - \omega_p + \omega) + 2(|p|^2 + |s|^2 + |i|^2) - |p|^2 \\ \bar{d}_p &= \frac{1}{|X_p|^2}(\omega_0(k_p + q) + i\gamma_p - \omega_p - \omega) + 2(|p|^2 + |s|^2 + |i|^2) - |p|^2 \end{aligned} \quad (13)$$

with equivalent expressions for d_s , \bar{d}_s etc. The terms in the determinant are, in order of the columns, the coefficients multiplying the amplitudes of the fluctuations in p , p^* , s , s^* , i and i^* .

In Fig.5 the eigenvalues calculated from Eq.12 are plotted. Fig.5(a) shows the real parts of the roots for all the calculated eigenmodes. The calculated energies, ω , are the excitations from the OPO state, which has three energies and wave-vectors (ω_p, k_p) , (ω_i, k_i) and (ω_s, k_s) . Thus, in a similar manner to the discussion concerning Eq.2, each excitation corresponds to six absolute energies and wave-vectors, $(k_p \pm q, \omega_p \pm \omega)$, $(k_s \pm q, \omega_s \pm \omega)$ and $(k_i \pm q, \omega_i \pm \omega)$. These are the values at which the excited states can be created from, or transformed into an external photon, and it is these energies and wave-vectors which are plotted on the figure. The resulting dispersion curves, which are highly complicated, could be observed as parametric luminescence in the presence of the OPO state; indeed, analogous features have been observed in ultrafast pump-probe measurements.¹³

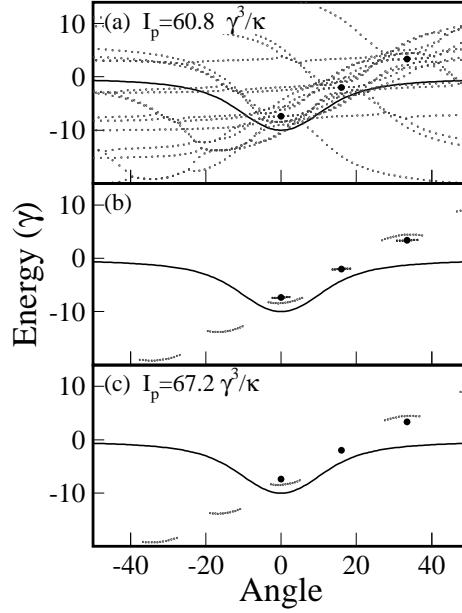


FIG. 5: Real part of dispersion curves for excitations from the OPO state with $\theta_p = 16^\circ$, $\omega_p = -2\gamma$ and $\theta_s = 0^\circ$. (a) shows all the branches for the unstable state with $I_p = 60.8\gamma^3/\kappa$, (b) the branches which are actually unstable. (c) shows the unstable branches for the nominally ‘stable’ state with $I_p = 67.2\gamma^3/\kappa$, as discussed in the text. The solid line is the bare polariton dispersion and the large points are the (θ, ω) locations of the pump, signal and idler.

Fig.5(b) shows only the modes which are unstable, that is $\text{Im}(\omega) > 0$. For this pump power there are two types of unstable excitation: small wave-vector modes, represented by the short, near horizontal, sections of dispersion passing through the pump, signal and idler, and much larger wave-vector modes which give rise to the longer arcs. For example, the long arc close to the idler is actually an excitation from the signal, with wave-vector $q \sim k_i - k_s$, and it is paired with the arc at $\sim -30^\circ$.

Fig.5(c) corresponds to a slightly higher pump power than (b), where the small wave-vector instability has disappeared. However the large wave-vector modes remain, and indeed are always found in the present calculations, suggesting that the simple OPO state is never really stable. In fact, this is known to be true: in the experiments of Tartakovskii *et al.*,¹² the OPO state is found to be accompanied by additional weak satellites, s' and i' , at $k_{s'} = 2k_s - k_p$ and $k_{i'} = 2k_i - k_p$, corresponding to the scattering processes $p + p \rightarrow s' + i'$, $s + i \rightarrow s' + i'$, $p + s \rightarrow s' + i$ and $p + i \rightarrow s + i'$. Such satellites can also be seen in the numerical simulations of Ref.(9). These particular states are selected because the corresponding q is equal to $k_p - k_s$, a resonance condition which is not accounted for in the derivation of Eq.12. However, the comparison suggest that the instability associated with the large wave-vector modes is benign, and does not grow very large before being limited by non-linear terms. Distinguishing such instabilities from the more catastrophic variety is not possible within a linear stability analysis of the type performed here, which only shows that an infinitesimally small fluctuation in one of these modes will initially grow.

Adopting the criterion that only the small wave-vector instabilities are important, Fig.6 shows the portions of the OPO curves with negative θ_s , in Fig.4(c), which are stable. It can be seen that for a particular pump power, the OPO state with the lowest pump population $|p|^2$ is stable. This is consistent with the discussion in Ref.(7), where it was argued that if a state with lower $|p|^2$ were possible, the higher $|p|^2$ state would be unstable. However, in the present treatment, the stable region for a particular angle extends beyond where it has lowest $|p|^2$. This is because stability is concerned with the response to infinitesimal fluctuations, and for a given pump power and signal angle, a small fluctuation in another mode may decay, where a large excursion into that mode would be stable.

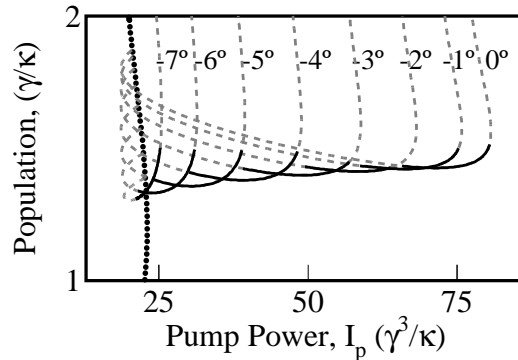


FIG. 6: Stable regions of $|p|^2$ versus I_p , for various signal angles θ_s , according to the criteria discussed in the text. The solid lines represent the stable states.

IV. DISCUSSION

The results presented in this paper show that a proper treatment of the polariton renormalisation leads to a model which predicts the pump conditions under which the microcavity OPO can be observed, and explains the tendency for the signal emission to be close to the surface normal at high pump powers.

The OPO threshold behaviour has been shown to be a consequence of how the mismatch in energy between the pump, signal and idler modes, Δ in Eq.6, changes when their energies are renormalised by the self-interaction terms. This suggests an explanation for the observation, in ultrafast pump-probe measurements, that the ‘magic-angle’ for pumping is important: when an external probe is used the energies and angles of all three modes are determined by the experimental geometry, so the system cannot re-arrange itself in the same way. Hence, a strong response is only obtained when the bare polariton dispersion is resonant with the three modes, which gives the magic-angle condition. Indeed, as CW experiments are always carried out with the pump positively detuned from the bare dispersion, it is probably not surprising that the triple resonance condition is not important.

The model also predicts that in the OPO region, there is a maximum pump power above which the OPO switches off, as well as a lower threshold. This behaviour is observed in numerical simulations such as Ref.(9), but not in experiments. This is probably a consequence of the inevitably inhomogeneous pump intensity associated with a finite excitation spot. A two dimensional numerical model¹⁰ with a Gaussian excitation profile shows that, as the power is turned up, the signal switches off at the centre of the spot, but there is always a region further out where the intensity is in the right range for the OPO to be active.

A further prediction is that for given pumping conditions, there are a number of stable OPO states corresponding to different signal angles. This suggests that the actual state obtained will depend on exactly how the OPO is switched on, and possibly on random factors such as noise in the system. It may also be possible to steer the signal, by using a second probe beam to favour a particular emission angle.

Acknowledgments

I wish to thank P. R. Eastham, D. Sanvitto and M. S. Skolnick for helpful contributions in discussions about this work. I also acknowledge the financial support of the EPSRC (GR/A11601)

¹ R. M. Stevenson, V. N. Astratov, M. S. Skolnick, D. M. Whittaker, M. Emam-Ismael, A. I. Tartakovskii, P. G. Savvidis, J. J. Baumberg and J. S. Roberts, Phys. Rev. Lett. **85** 3680 (2000).

² J. J. Baumberg, P. G. Savvidis, R. M. Stevenson, A. I. Tartakovskii, M. S. Skolnick, D. M. Whittaker and J. S. Roberts Phys. Rev. B **62** R16247 (2000).

- ³ R. Butté, M. S. Skolnick, D. M. Whittaker, D. Bajoni and J. S. Roberts, Phys. Rev. B **68** 115325 (2003).
- ⁴ P. G. Savvidis, J. J. Baumberg, R. M. Stevenson, M. S. Skolnick, D. M. Whittaker and J. S. Roberts, Phys. Rev. Lett. **84** 1547 (2000).
- ⁵ J. Erland, V. Mizeikis, W. Langbein, J. R. Jensen, and J. M. Hvam Phys. Rev. Lett. **86** 5791 (2000).
- ⁶ C. Ciuti, P. Schwendimann, B. Deveaud and A. Quattropani, Phys. Rev. B **62**, R4825 (2000).
- ⁷ D. M. Whittaker, Phys. Rev. B **63** 193305 (2001).
- ⁸ A. Baas, J. Ph. Karr and E. Giacobino, cond-mat/0306473 (2003).
- ⁹ N. A. Gippius, S. G. Tikhodeev, V. D. Kulakovskii, D. N. Krizhanovskii and A. A. Tartakovskii, cond-mat/0312214 (2003).
- ¹⁰ D. M. Whittaker, unpublished results.
- ¹¹ In this, and all other numerical results, the the relative detuning of the exciton and cavity is zero at $k = 0$. The coupling strength is chosen to be 20 times the line-width, a typical value for the good GaAs microcavities studied experimentally.
- ¹² A. I. Tartakovskii, D. N. Krizhanovskii, D. A. Kurysh, V. D. Kulakovskii, M. S. Skolnick and J. S. Roberts Phys. Rev. B **65** 081308 (2002)
- ¹³ P. G. Savvidis, C. Ciuti, J. J. Baumberg, D. M. Whittaker, M. S. Skolnick and J. S. Roberts Phys. Rev. B **64** 075311 (2001)